PROCEEDINGS

2020 7th International Congress on Energy Fluxes and Radiation Effects (EFRE)

Tomsk, Russia, September 14 – 26, 2020

SPONSORED BY

IEEE Nuclear and Plasma Sciences Society

Institute of High Current Electronics of the Siberian Branch of the Russian Academy of Sciences

National Research Tomsk Polytechnic University

Tomsk Scientific Center of the Siberian Branch of the Russian Academy of Sciences

Chairman

Nikolay Ratakhin
Institute of High Current Electronics, Tomsk, Russia

Co-Chairman

Andrey Yakovlev
National Research Tomsk Polytechnic University, Tomsk, Russia

Alexey Markov
Tomsk Scientific Center SB RAS, Tomsk, Russia

Program Chairman

Alexander Batrakov
Institute of High Current Electronics, Tomsk, Russia

Program Co-Chairman

Edl Schamiloglu
University of New Mexico, Albuquerque, USA

Accumulation and Annealing of Radiation Donor Defects in Arsenic-Implanted $Hg_{0.7}Cd_{0.3}Te$ Films

Alexandr Voitsekhovskii
Tomsk State University
36 Lenin, 634050
Tomsk, Russia
vav43@mail.tsu.ru

Alexandr Korotaev
Tomsk State University
36 Lenin, 634050
Tomsk, Russia

Ihor Izhnin
Scientific Research Company “Electron-Carat”
202 Stryysyka Str., 79031
Lviv, Ukraine
i.izhnin@carat.electron.ua

Karim Mynbaev
Ioffe Institute
26 Polytechnicheskaya Str., 194021
Saint-Petersburg, Russia
mynkad@mail.ioffe.ru

Maxim Yakushev
A.V. Rzhanov Institute of Semiconductor Physics SB RAS
13 Ac. Lavrentieva, 630090
Novosibirsk, Russia

Nikolaj Mikhailov
A.V. Rzhanov Institute of Semiconductor Physics SB RAS
13 Ac. Lavrentieva, 630090
Novosibirsk, Russia

Vasilij Varavin
A.V. Rzhanov Institute of Semiconductor Physics SB RAS
13 Ac. Lavrentieva, 630090
Novosibirsk, Russia

Sergej Dvoretsky
A.V. Rzhanov Institute of Semiconductor Physics SB RAS
13 Ac. Lavrentieva, 630090
Novosibirsk, Russia

Denis Marin
A.V. Rzhanov Institute of Semiconductor Physics SB RAS
13 Ac. Lavrentieva, 630090
Novosibirsk, Russia
yakushev@isp.nsc.ru

Olena Fitsych
P. Sagaidachny National Army Academy
32 Gvardijska Str., 79012
Lviv, Ukraine
o_fitsych@ukr.net

Kurban Kurbanov
Kremenchug Flight College
17 Pobedy Str., 39600
Kremenchug, Ukraine
kurbanovkurban424@gmail.com

***Abstract*—Processes of accumulation and annealing of radiation-induced donor defects in arsenic-implanted $Hg_{0.7}Cd_{0.3}Te$ films were studied with the use of the Hall-effect measurements with processing the data with mobility spectrum analysis. A substantial difference in the effects of arsenic implantation and post-implantation activation annealing on the properties of implanted layers and photodiode ‘base’ layers in $Hg_{0.7}Cd_{0.3}Te$ and $Hg_{0.8}Cd_{0.2}Te$ films was established and tentatively explained.**

***Keywords*—HgCdTe, implantation, defects.**

I. Introduction

$Hg_{1-x}Cd_xTe$ (MCT) solid solutions have remained one of the basic materials of the infrared (IR) photo-electronics for the last 60 years [1]. In the last 20 years, the ‘p^+–n’-type MCT-based photodiodes have become increasingly popular due to their ability to provide better operation at higher temperatures or longer cut-off wavelengths than those of traditional ‘n^+–p’-type MCT devices [2]. The most common method of the fabrication of a p^+–layer in an n–type MCT ‘base’ layer with the aim of the development of a ‘p^+–n’-junction is ion implantation of arsenic followed by a two-stage activation annealing. The latter treatment is used for the annealing of implantation-induced defects and for the electrical activation of the implanted arsenic ions. Fabrication of the photodiodes with ultimate parameters requires understanding of the processes of accumulation and annealing of the radiation-induced defects. Studies of these processes were performed earlier on MCT films with the composition of the photosensitive ‘active’ layer $x_a \approx 0.22$; this material serves as a basis for the fabrication of long-wavelength IR photodiodes [3]. In this work, we report on the results of similar studies performed on MCT films with $x_a \approx 0.30$; this material is suitable for the development of middle-wavelength IR (MWIR) devices. MWIR range is a home to the spectral peak of the thermal emission signatures of many biological and mechanical objects with temperatures from 200 K an up, and for this reason is of vital importance for security, defense, energy auditing applications, medicine, etc.

This research was supported by Ministry of Science and Higher Education of the Russian Federation, project No 0721-2020-0038.

978-1-7281-2685-2/20/$31.00 ©2020 IEEE

II. EXPERIMENTAL DETAILS

The studies were performed on films with *p*– (due to the presence of mercury vacancies, acceptors in MCT) and *n*–type conductivity of the photodiode 'base' layers. The films were grown at Rzhanov Institute of Semiconductor Physics (Novosibirsk, Russia) by Molecular Beam Epitaxy (MBE) on GaAs and Si substrates with *in situ* ellipsometric control over their thickness and composition [4]. The 'active' layers of the films with $x_a \approx 0.30$ were covered with graded-gap surface layers (GSL) with composition at the surface $x_s \approx 0.45$. Arsenic implantation was performed with ion energies $E = 190$ keV and $E = 350$ keV and ion fluences ranging from 10^{12} to 10^{15} cm^{-2} with the use of IMC200 (Ion Beam Services, France) machine. The electrical characterization of the implanted films was performed by studying the magnetic field B dependences of the Hall coefficient $R_H(B)$ and conductivity $\sigma(B)$ at the temperature $T = 77$ K. The experimental data were processed with the discrete mobility spectrum analysis (DMSA), which allowed for obtaining the information on the sets of carriers present in the samples and their parameters: average concentration, mobility and partial conductivity [3].

III. RESULTS AND DISCUSSION

The objects of the study were *p*-type samples M14 and M15 (hole concentration ~ 10^{16} cm^{-3}, hole mobility ~ 400 cm^2/(V·s)) and *n*-type samples M16 and M17 (electron concentration ~ 10^{14} cm^{-3}, electron mobility ~ 40000 cm^2/(V·s)) with very similar x_a. Fig. 1 shows the dependences of the total, experimentally measured, conductivity of the implanted *p*-type samples on the ion fluence. The experimental results obtained in this work are complemented in this figure with the data obtained earlier on the material with $x_a \approx 0.22$ [5]. It is known that after ion implantation in MCT the conductivity is typically dominated by low-mobility electrons originating in the defects that were induced by radiation damage [3,5]. As follows from Fig. 1, for samples with $x_a \approx 0.30$ the increase in conductivity with the fluence increasing was not that steep than that for samples with $x_a \approx 0.22$. With the exception of sample M14 implanted with $E = 190$ keV, the conductivity in samples with $x_a \approx 0.30$ experienced saturation when fluencies exceeded 10^{13} cm^{-2}.

Fig. 2 shows the transformation of the primary envelopes of the mobility spectra with the increase in ion fluence for sample M14 implanted with $E = 190$ keV. These data clearly show the dominating contribution to the conductivity of the low-mobility electrons: the strongest peak in the spectra is that of these electrons; it stands near to zero mobility axis (the negative part of the axis was introduced for demonstration purposes only, so that mobility peaks corresponding to electrons and holes would not superimpose).

Fig. 3 shows the transformation of the primary envelopes of the mobility spectra with the increase in ion fluence for the same sample implanted with $E = 350$ keV. In this case, the amplitude of the peak corresponding to the conductivity of the low-mobility electrons changed insignificantly with fluence increasing. This was indicative of the saturation of the concentration of radiation-induced defects that were responsible for the appearance of the low-mobility electrons in the implanted material. For arsenic ion energy $E = 190$ keV, with fluence increasing, the amplitude of the peak corresponding to the low-mobility electrons increased and showed no sign of saturation (Fig. 2). This result agrees well with the data on the dependence of the integral conductivity on the ion fluence presented in Fig. 1. With few exceptions, none of the primary mobility spectra envelopes of implanted samples showed the presence of the electrons with mid-mobility, which were typical of arsenic-implanted MCT with $x_a \approx 0.22$ [3, 5]. In samples with $x_a \approx 0.30$, these electrons were detected only in secondary mobility spectra envelopes that were obtained after discretization.

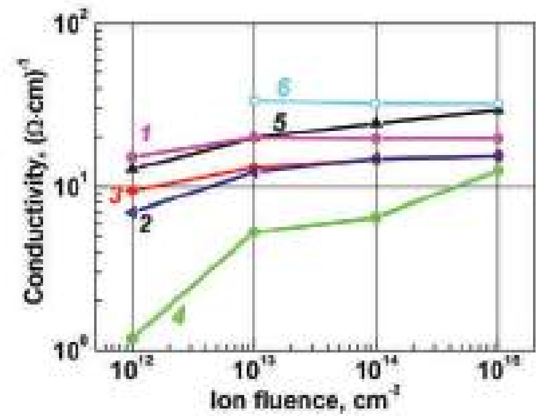

Fig. 1. Fluence dependences of total conductivity for samples M15 (*1*, *2*) and M14 (*3*, *4*) implanted with ion energies E=350 keV (*1*, *3*) and E=190 keV (*2*, *4*), respectively. Data *5* and *6* show similar dependences for one and the same sample with x_a≈0.22 with (*5*) and without (*6*) GSL implanted with E=190 keV.

Fig. 4 shows the dependence of the partial conductivity provided by the low-mobility electrons on the ion fluence. The data again are complemented with the results obtained for MCT sample with $x_a \approx 0.22$ and are shown for the partial conductivity provided by the low-mobility electrons as reduced to the total thickness of the MCT structure. In our *p*-type samples we observed rather weak dependence of the partial conductivity on the ion fluence. The saturation effect was observed at fluences as low as 10^{13} cm^{-2}. In samples with $x_a \approx 0.22$ the saturation was not observed at fluences as high as 10^{15} cm^{-2} [5]. In [5], we have noted the difference in the behavior of the ion fluence dependences of the concentration and partial conductivity of the low-mobility electrons in samples with $x_a \approx 0.22$ with GSL intact and removed. It was suggested that this difference was due to the effect of the built-in internal electric field of GSL. This field strongly affects the diffusion of charged defects, which is illustrated in Fig. 1 for an MCT sample with $x_a \approx 0.22$: as can be seen in this figure, the dynamics of accumulation of defects in sample with GSL (curve *5*) was very different from that in the same sample with GSL removed with chemical etching (curve *6*), which is clearly indicative of the strong effect of this layer. In MCT samples with $x_a \approx 0.30$ the value of the internal electric field would be smaller than that in samples with $x_a \approx 0.22$ with similar x_s, so the effect of this field on the dynamics of accumulation of implantation-induced defects should be weaker, too.

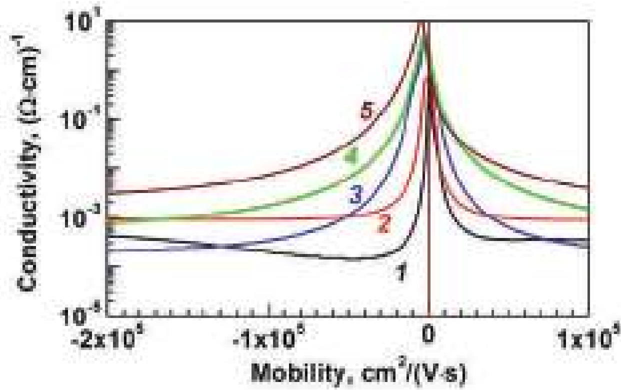

Fig. 2. Primary mobility spectra envelopes for film M14 implanted with arsenic ion energy E=190 keV: *1*, as-grown film, and *2*, *3*, *4* and *5*, samples implanted with fluences 10^{12}, 10^{13}, 10^{14}, and 10^{15} cm^{-2}, respectively. Activation annealing was not performed.

The concentration of the low-mobility electrons in samples M14 and M15 implanted with $E = 190$ keV, as reduced to a ~ 0.3 μm-thick layer equaled (3–5)·10^{17} cm^{-3}. In these samples implanted with $E = 350$ keV it equaled (3–4.5)·10^{17} cm^{-3} (in a ~ 0.5 μм-thick layer). For comparison, in MCT with $x_a \approx 0.22$ implanted with $E = 190$ keV the concentration of these electrons for fluences 10^{12}–10^{15} cm^{-2} also equaled (3–7)·10^{17} cm^{-3}. For boron implantation with E=100 keV and fluences 10^{13}–10^{15} cm^{-2}, the concentration of the low-mobility electrons in samples with $x_a \approx 0.30$ equaled 10^{18} cm^{-3} [6].

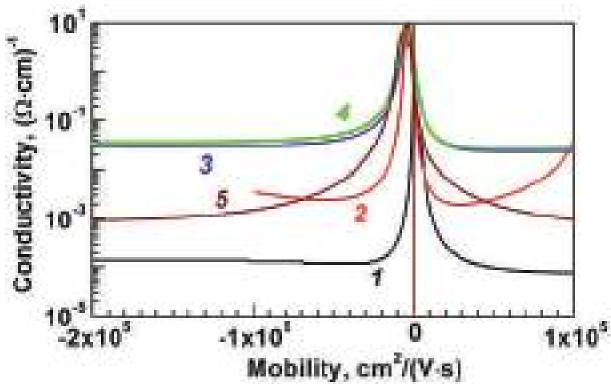

Fig. 3. Primary mobility spectra envelopes for film M14 implanted with arsenic ion energy $E = 350$ keV: *1*, as-grown film, and *2*, *3*, *4* and *5*, samples implanted with fluences 10^{12}, 10^{13}, 10^{14}, and 10^{15} cm^{-2}, respectively. Activation annealing was not performed.

DMSA showed that in most of the arsenic-implanted *p*-type samples with $x_a \approx 0.30$ the major contributions to conductivity were those by the mid-mobility electrons (10000–15000 cm^2/(V·s)) and low-mobility electrons (2500–4000 cm^2/(V·s)). Thus, an n^+–p structure was formed as a result of implantation. Only in one of the implanted *p*-type samples the high-mobility electrons (20000–30000 cm^2/(V·s)) were found. Thus, in this sample, an n^+–n–p structure was formed, which is in general typical of arsenic-implanted samples with $x_a \approx 0.22$ [5].

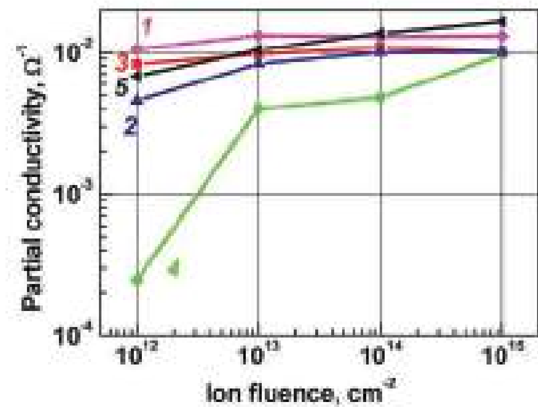

Fig. 4. Fluence dependences of partial conductivity provided by the low-mobility electrons for samples M15 (*1*, *2*) and M14 (*3*, *4*) implanted with $E = 350$ keV (*1*, *3*) and $E = 190$ keV (*2*, *4*), respectively. Data *5* show similar dependence for a sample with $x_a \approx 0.22$ (with GSL) implanted with $E = 190$ keV.

Fig. 5 shows the transformation of the primary envelopes of the mobility spectra for *n*-type sample M16 implanted with energies $E = 190$ keV and $E = 350$ keV and subjected to arsenic activation annealing. In the as-grown sample the major contribution to conductivity was that by the majority carriers of the 'active' layers, i.e., the high-mobility electrons (curve *1*). After the implantation, the conductivity was dominated by the low-mobility electrons originated in donor defects induced by implantation (curves *2* and *4*); still, high-mobility electrons were also present. After the post-implantation annealing, the mobility peak due to the low-mobility electrons disappeared (curves *3* and *5*), which was indicative of the annihilation of the implantation-induced defects. At the same time, curves *3* and *5* demonstrated mobility peaks near the 'zero' mobility value. This was indicative of the appearance of hole mobility due to the electrical activation of the implanted arsenic ions. The primary envelopes of the mobility spectra of sample M17 were very similar to those of sample M16.

DMSA of the as-implanted *n*-type samples showed the presence of three sorts of electrons that contributed to the conductivity. These were the low-mobility electrons with the mobility of the order 3000–5000 cm^2/(V·s), which provided the dominating contribution to the conductivity, the high-mobility electrons with the mobility 50000–60000 cm^2/(V·s), and the mid-mobility electrons with the mobility 14000–20000 cm^2/(V·s), which provided the lowest contribution to the conductivity. For example, in sample M16 implanted with $E = 190$ keV, the conductivity was dominated by the low-mobility electrons with average concentration 8.90·10^{15} cm^{-3} and mobility 4080 cm^2/(V·s). The next sort of carriers detected with DMSA was the high-mobility electrons with average concentration 1.47·10^{14} cm^{-3} and mobility 60800 cm^2/(V·s) (interestingly, the mobility of these electrons was twice as high as that in the as-grown sample). The mid-mobility electrons were also found in the implanted sample, their average concentration equaled 2.75·10^{14} cm^{-3}, mobility,

19600 cm^2/(V·s). Thus, arsenic implantation into *n*-type $Hg_{0.7}Cd_{0.3}Te$ films, similar to the case of $Hg_{0.8}Cd_{0.2}Te$ films, resulted in the formation of n^+–*n*–structure. In this structure, the *n*–layer represents the material that was not affected by the implantation, while the formation of the n^+–layer is the direct result of the implantation. The parameters of the electrons of the *n*-layer in $Hg_{0.7}Cd_{0.3}Te$ films, in contrast to $Hg_{0.8}Cd_{0.2}Te$ films, strongly differed from those in as-grown samples. The average electron concentration and partial conductivity in as-implanted samples were twice as high as in as-grown ones. In MBE-grown MCT, these carriers originate both in the implantation-induced defects and in defects located at the transitional 'epitaxial film/CdTe buffer' layer [7]. A similar assortment of carriers was observed in other implanted samples, including samples studied in this work and samples with $x_a \approx 0.22$ studied in [3, 5].

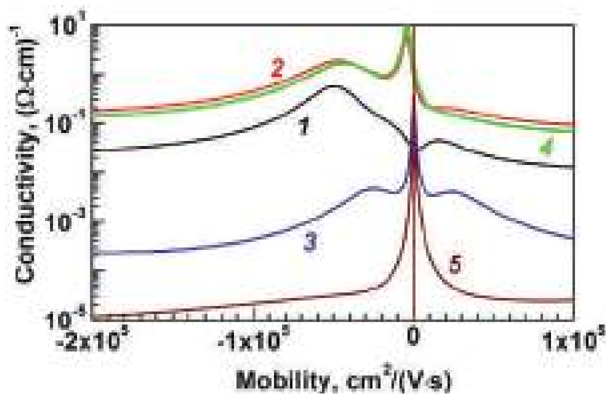

Fig. 5. Primary mobility spectra envelopes for film M16: *1,* as-grown film; *2*, after implantation with $E = 190$ keV; *3*, after activation annealing of sample implanted with $E = 190$ keV; *4*, after implantation with $E = 350$ keV; *5*, after activation annealing of sample implanted with $E = 350$ keV.

DMSA of the implanted and annealed *n*-type samples also showed some difference in the behavior of films with $x_a \approx 0.30$ and $x_a \approx 0.22$. While for the latter (and similar indium-doped or un-doped MCT samples) the major contribution to conductivity was that by the high-mobility electrons of the *n*-type 'base' layer, in samples with $x_a \approx 0.30$ the conductivity was dominated by the heavy holes. In fact, for all the implanted and annealed *n*-type samples studied in this work, the contribution to conductivity by the high-mobility electrons could not be detected at all. The degree of the electrical activation of arsenic after the annealing, though, appeared to be low, ~ 0.3 for sample M16 and just ~ 0.1 for sample M17, almost irrespective of ion energy. In indium-doped samples with $x_a \approx 0.22$ the degree of the electrical activation of arsenic was much higher and close to 0.7. Currently, there is no explanation for the low degree of arsenic activation in the samples studied in this work; this matter requires further investigation.

What is important is that after the annealing the mobility peak corresponding to the low-mobility (~ 3500–4500 cm^2/(V·s)) electrons, which was clearly seen straight after the implantation (curves *2* and *4* in Fig. 5), completely disappeared (curves *3* and *5* in Fig. 5). As the electrons with low mobility in such samples originate in the atoms of interstitial mercury captured by dislocation loops [3, 5], and these electrons are localized in the layer containing extended defects, their disappearance after the annealing is due to the annealing of the defects. A similar conclusion was made on the basis of the data acquired during the reflectance studies of the implanted and annealed samples with $x_a \approx 0.30$ [8]. The concentration of the mid-mobility electrons, which doubled and even tripled after the implantation, significantly dropped (down to ~ 10^{12} см$^{-3}$) after the annealing. This was clearly indicative of the annealing of quasi-point implantation-induced defects that are supposedly responsible for the appearance of these electrons in arsenic-implanted MCT [3,5]. One of the important tasks of the activation annealing consists in keeping the properties of the 'base' layer of the photodiode as close to the original those as possible. Since during the first, high-temperature stage of the annealing a large number of mercury vacancies is generated in the material, the properties of the 'base' get inevitably changed (as mentioned above, mercury vacancies are intrinsic acceptors in MCT). The second, low-temperature stage of the annealing should restore the properties of the base by filling the vacancies; this is why it is performed under saturated mercury pressure. The exact effect of the low-temperature stage of the annealing on the properties of *n*-type 'base' of implanted MCT has not been studied in detail; however, it is always expected that this type of annealing should restore the original properties of the base, provided it was doped with indium with concentrations $5{\cdot}10^{14}$–$5{\cdot}10^{15}$ cm^{-3} (see, e.g., [2]).

In this work, however, we did not observe the restoration of the parameters of the *n*-type 'base' after the activation annealing. DMSA did not reveal any high-mobility electrons in our samples with $x_a \approx 0.30$ after the annealing, which contrasts the current results with those obtained earlier on indium-doped samples with $x_a \approx 0.22$ [3,5]. Thus, in *n*-type samples with $x_a \approx 0.30$ after the implantation and the annealing an p^+-(*n*)–structure was formed, where p^+–layer was formed by the implanted and activated arsenic ions with heavy hole concentration much smaller than the averaged concentration of the ions. The *n*–layer of this structure, in its turn, was formed by the mid-mobility electrons of the transitional "epitaxial film/CdTe buffer" layer. Therefore, the parameters of the *n*–type 'base' were somehow modified by the annealing and did not return to their original values as required by the 'p^+–*n*'-photodiode architecture.

IV. Conclusion

In our study of MBE-grown *p*-type HgCdTe films with $x_a \approx 0.30$ implanted with arsenic (and not annealed) we observed formation of 'n^+–*p*' structures (not 'n^+–*n*–*p*' structures typical of films with $x_a \approx 0.22$). The dominating (~ 80%) contribution to conductivity in the implanted samples was that by the low-mobility (2500–4000 cm^2/(V·s)) electrons originated in donors possibly related to the interstitial mercury captured by the implantation-induced dislocation loops. The next, much lower, contribution was that by the mid-mobility (10000–15000 cm^2/(V·s)) electrons originated in the interstitial mercury captured by the implantation-induced quasi-point defects. In contrast to samples with $x_a \approx 0.22$, in samples with $x_a \approx 0.30$ we observed weak dependences of partial

conductivity provided by the low-mobility electrons on ion fluence; at 10^{13} cm^{-2} fluence, a saturation of the dependence was observed. It was suggested that this difference is caused by the different effect of the built-in electric field of GSL in samples with $x_a \approx 0.30$ and $x_a \approx 0.22$ with x_s being similar and equaling 0.45. The degree of the electrical activation of implanted arsenic as a result of the annealing in originally *n*-type samples with $x_a \approx 0.30$ appeared to be much lower than that in samples with $x_a \approx 0.22$. Also, in contrast to the latter, the annealing performed in this work did not result in the restoration of the electrical properties of the *n*-type 'base' of the photodiode structures. These effects may be related to the different impurity backgrounds in samples with $x_a \approx 0.30$ and $x_a \approx 0.22$ and requires further investigation.

Acknowledgment

This research was supported by Ministry of Science and Higher Education of the Russian Federation, project No 0721-2020-0038.

References

[1] R. K. Bhan and V. Dhar, "Recent infrared detector technologies: applications, trends and development of HgCdTe based cooled infrared focal plane arrays and their characterization," *Opto-Electron. Review*, vol. 27, pp. 174–193, June 2019.

[2] L. Mollard, G. Bourgeois, C. Lobre, et al., "*P*-on-*n* HgCdTe infrared focal-plane arrays: from short-wave to very-long-wave infrared," *J. Electron. Mater.*, vol. 43, pp. 802–807, March 2014.

[3] I. I. Izhnin, K.D. Mynbaev, A.V. Voitsekhovsky, et al., "Arsenic-ion implantation-induced defects in HgCdTe films studied with Hall-effect measurements and mobility spectrum analysis," *Infr. Phys. Technol.*, vol. 98, pp. 230–235, May 2019.

[4] M. V. Yakushev, D. V. Brunev, V. S. Varavin, V. V. Vasilyev, S. A. Dvoretskii, I. V. Marchishin, et al., "HgCdTe heterostructures on Si(310) substrates for MWIR infrared photodetectors," *Semiconductors*, vol. 45, pp. 385–391, March 2011.

[5] I. I. Izhnin., A. V. Voitsekhovsky, A. G. Korotaev, et al., "Optical and electrical studies of arsenic–implanted HgCdTe films grown with molecular beam epitaxy on GaAs and Si substrate," *Infr. Phys. Technol.*, vol. 81, No 3, pp. 52–58, March 2017.

[6] A. V. Voitsekhovskii, D. V. Grigoryev, A. G. Korotaev, et al., "Influence of composition of $Hg_{1-x}Cd_xTe$ (x=0.22-0.57) epitaxial film on dynamics of accumulation and spatial distribution of electrically active radiation defects after boron implantation," *Mater. Res. Express.*, vol. 6, No 7, Art. no. 075912, April 2019.

[7] V. S. Varavin, A. F. Kravchenko, and Yu. G. Sidorov, "A Study of Galvanomagnetic Phenomena in MBE-Grown n-$Cd_xHg_{1-x}Te$ Films," *Semiconductors*, vol. 32, pp. 992–996, September 2001.

[8] O. Yu. Bonchyk, H. V. Savytskyy, I. I. Izhnin, et al., "Nano-size defect layers in arsenic-implanted and annealed HgCdTe epitaxial films studied with transmission electron microscopy," *Appl. Nanosci.*, 2020, DOI: 10.1007/s13204-020-01327-9